Tailoring the Vapor–Liquid–Solid Growth toward the Self-Assembly of GaAs Nanowire Junctions

ARTICLE *in* NANO LETTERS · OCTOBER 2011

Impact Factor: 13.59 · DOI: 10.1021/nl202888e · Source: PubMed

7 AUTHORS, INCLUDING:

Shadi A Dayeh
University of California, San Diego
104 PUBLICATIONS **3,605** CITATIONS
SEE PROFILE

Jian Wang
University of Nebraska at Lincoln
153 PUBLICATIONS **1,440** CITATIONS
SEE PROFILE

Haibin Su
Nanyang Technological University
175 PUBLICATIONS **2,020** CITATIONS
SEE PROFILE

NANO LETTERS

LETTER

pubs.acs.org/NanoLett

Tailoring the Vapor−Liquid−Solid Growth toward the Self-Assembly of GaAs Nanowire Junctions

Xing Dai,[†] Shadi A. Dayeh,[‡] Vaithianathan Veeramuthu,[†] Alexandre Larrue,[⊥] Jian Wang,[§] Haibin Su,[⊥,∥] and Cesare Soci*[,†,⊥,#]

[†]Division of Physics and Applied Physics, 21 Nanyang Link, Nanyang Technological University, Singapore 637371

[‡]Center for Integrated Nanotechnologies and [§]Materials Science and Technology, Los Alamos National Laboratory, Los Alamos, New Mexico 87545, United States

[⊥]CINTRA CNRS/NTU/THALES, UMI 3288, Research Techno Plaza, 50 Nanyang Drive, Border X Block, Level 6, Singapore 637553

[∥]Division of Materials Science and [#]Division of Microelectronics, 50 Nanyang Avenue, Nanyang Technological University, Singapore 639798

Supporting Information

ABSTRACT: New insights into understanding and controlling the intriguing phenomena of spontaneous merging (kissing) and the self-assembly of monolithic Y- and T-junctions is demonstrated in the metal−organic chemical vapor deposition growth of GaAs nanowires. High-resolution transmission electron microscopy for determining polar facets was coupled to electrostatic−mechanical modeling and position-controlled synthesis to identify nanowire diameter, length, and pitch, leading to junction formation. When nanowire patterns are designed so that the electrostatic energy resulting from the interaction of polar surfaces exceeds the mechanical energy required to bend the nanowires to the point of contact, their fusion can lead to the self-assembly of monolithic junctions. Understanding and controlling this phenomenon is a great asset for the realization of dense arrays of vertical nanowire devices and opens up new ways toward the large scale integration of nanowire quantum junctions or nanowire intracellular probes.

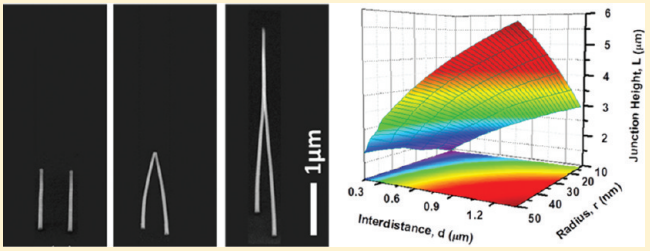

KEYWORDS: Vapor−liquid−solid growth mechanism, monolithic nanowire junctions, transmission electron microscopy, polar interactions, electrostatic−mechanical modeling, nanowire arrays

Semiconductor nanowires (NWs) are widely considered for the development of optoelectronic functional systems where large sensitivity,[1−3] dense integration,[4,5] and complex polymorphic heterostructures[4,6−9] are desired. III−V NWs are among the best candidates for NW-based optoelectronics thanks to their direct bandgap, versatility in band gap engineering, and high electron mobility.[10−13] Growth of vertical and dense arrays of NWs at predefined positions is a superior method for large scale integration when compared to available NW transfer methods to host substrates, such as the Langmuir−Blodgett,[14] blown bubble film,[15] direct printing,[5] or electrochemical deposition methods.[16] Selective-position arrays are conventionally fabricated combining high-resolution lithography (such as electron beam,[4] nanoimprint,[17] or interference[18] lithography) with chemical vapor deposition methods for NW growth. The underlying assumption is that dense vertical NW arrays are stable structures, irrespective of their integration density or pitch. This is generally acceptable because nanoscale mechanical forces tend to overcome those due to surface energy minimization or electrostatic interactions between charged surfaces on adjacent NWs. However, as the energy scale of these forces becomes comparable to that of mechanical forces, their influence on the growth mechanism and the resulting morphology of nanostructures becomes significant.

In the case of the vapor−liquid−solid (VLS) growth of III−V NWs,[19,20] the attraction of spontaneously induced polar surfaces can result in the merging of vertical NWs during (in situ) or after (ex-situ) their growth,[21,22] a phenomenon that is hereby referred to as "nanowire kissing". While making the synthesis of faultless, dense arrays of individual nanowires a challenge, NW kissing can be regarded as an additional degree of freedom in the bottom-up VLS paradigm to realize functional nanostructures with greater complexity.

GaAs NWs were grown by metal−organic chemical vapor deposition (MOCVD) in a horizontal reactor (Aixtron 200). Epitaxial growth was obtained on GaAs (111)B substrates using Au nanoparticles as the growth seeds and trimethyl-gallium (TMGa) and tertiary-butyl-arsine (TBAs) as metal−organic precursors in hydrogen carrier gas. In this study the TMGa, TBAs, and total molar flow rates were 0.91, 12.91, and 2.30 μmol/s,

Received: August 20, 2011
Revised: September 22, 2011

   dx.doi.org/10.1021/nl202888e | *Nano Lett.* XXXX, XXX, 000–000

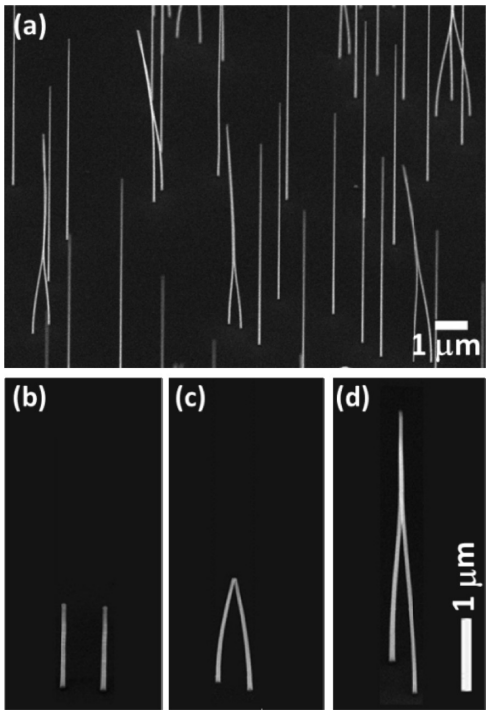

Figure 1. Nanowire kissing. (a) Vertical growth of individual GaAs NWs and merged NW bundles coexisting in the same substrate region. (b−d) Evolution of GaAs NW kissing observed from three individual growth runs with increasingly longer growth times (NW lengths): (b) two vertical NWs grow parallel to each other (t_g = 1 min); (c) NWs bend and kiss (t_g = 2 min); and (d) NWs merge in a bundle (t_g = 3 min). Tilted SEM images obtained at 45° angle.

respectively, corresponding to a V/III ratio of 14.25. The substrate temperature was set to 430 °C, and the reactor pressure was kept at 50 mbar during the growth. Growth time varied from t_g = 1 to 3.5 min. Comparable growth parameters are known to yield optimal GaAs NW morphology with reduced tapering.[23,24] NW kissing was observed for randomly dispersed Au nanoparticles (Ted Pella, Inc.) with diameters of 10−40 nm and was systematically studied using electron beam lithography (JEOL JSM-6600 equipped with a RAITH writer) for patterning arrays of Au discs with mask diameters of 45−90 nm and thickness of 15 nm, yielding NW diameters of 40−85 nm.

Morphological and structural characterization was performed via scanning electron microscopy (SEM, JEOL JSF-6700F, 5 keV acceleration voltage) and high-resolution transmission electron microscopy (HR-TEM, 300 keV FEI Tecnai F30). Specimens for the observation of individual NWs and junctions were prepared by ultrasonic dispersion of the GaAs NWs in ethanol for 5 s and by drop casting on glass slides or lacey TEM grids.

Figure 1a shows a typical array of vertical GaAs NWs grown from randomly dispersed Au nanoparticles. Surprisingly, both individual and merged NWs are observed within the same substrate area. The GaAs NWs maintain the [111] epitaxial relationship with the (111)B GaAs substrate, consistent with previous reports using similar growth conditions.[25] The NWs in Figure 1a have an average length of 8 μm with ∼70 nm diameter at their bases and ∼40 nm at their tip.

Merged NWs consist primarily of a bundle of two wires with separate bases (nucleation points) and common stems as a result of mutual attraction. As observed in Figure 1a, NWs that are sufficiently close to each other tend to merge together and form stable bundles. This phenomenon is repeatable and was observed in more than 30 independent growth runs. The formation of NW bundles could happen at any time during or after the growth, provided the NWs reach a critical length that allows them to bend and merge. Interestingly, observation by SEM was also found to induce NW kissing upon exposure to the electron beam (the Supporting Information video shows two vertical NWs merging during SEM observation). Although possible effects related to the electron beam bombardment, such as electrostatic charging or ablation of the native oxide layer from the exposed NW surfaces cannot be ruled out, NW kissing is likely to stem from the forced oscillations induced by the SEM beam which creates an instability bringing the two NWs closer together, to the point where attraction is favored. It is noteworthy that forced oscillations induced by the electron beam are a common and well-known effect during the observation of thin NWs by SEM, and the merging of two parallel InP NW tips[26] or neighboring GaAs NWs[22] was attributed to charging effects during SEM inspection in previous reports.

Repeated runs with the same growth parameters but different nanoparticle sizes and surface densities have been conducted to gain deeper understanding of the phenomenon and showed that kissing is favored for NWs with smaller diameters (due to their larger flexibility) and for larger nanoparticle surface densities (closer NW proximity). To elucidate the dynamics of NW kissing, several NW growths were conducted in identical conditions but with different growth times. Typical results for ∼40 nm diameter NWs growing at an average distance of 0.3 μm after 1, 2, and 3 min are also displayed in Figure 1. Within the first minute of growth, nucleation takes place, and the two NWs grow parallel to each other along the ⟨111⟩ direction (Figure 1b). As the NW length approaches ∼1.6 μm, e.g., after 2 min of growth, the two NWs begin to bend toward each other and eventually kiss, as observed after 3 min growth time (Figure 1c); at this point the VLS growth of the two NWs can either proceed independently, with two distinct NWs merging in a bundle after the point of contact, or the two liquid gold nanoparticles atop the NWs can fuse together, continuing to grow as a single stem after the point of contact (Figure 1c). For NWs nucleated from smaller nanoparticles (with diameters of 20 or 10 nm), kissing and merging were also observed, but due to the increased flexibility of the thinner NWs, the elevation of the point of contact relative to the substrate decreases and the maximum separation at which the branches can merge increases.

High-resolution transmission electron microscopy (HRTEM) characterization shows that both NWs have a zinc blende crystal structure (see inset FFT patterns in Figure 2b) with a few stacking faults observed throughout their length. Clear {111} lattice fringes are observed, marked by yellow (111), and orange ($\overline{1}\overline{1}1$) dashed lines. The stacking fault marked by the white arrow in Figure 2b leads to a 60° rotation of the (111) plane around the NW axis (Figures 2a and c). Figure 2d shows facets oriented in the ⟨112⟩ direction with a stepped structure of polar {111} and {113} planes[6] that correspond to the lowest calculated surface energies.[27] Interestingly, we observe in Figure 2d a surface nucleated Σ3(111) coherent twin boundary, consistent with prior observation for Si NWs.[28] The model in panels (e−g) shows a reconstruction of the faceted NWs from top (Figure 2e) and side ⟨110⟩ views (Figure 2f) and the configuration of two adjacent faceted NWs for kissing (Figure 2g). The considerable strength of the interaction responsible for NW kissing at microscopic

dx.doi.org/10.1021/nl202888e |*Nano Lett.* XXXX, XXX, 000–000

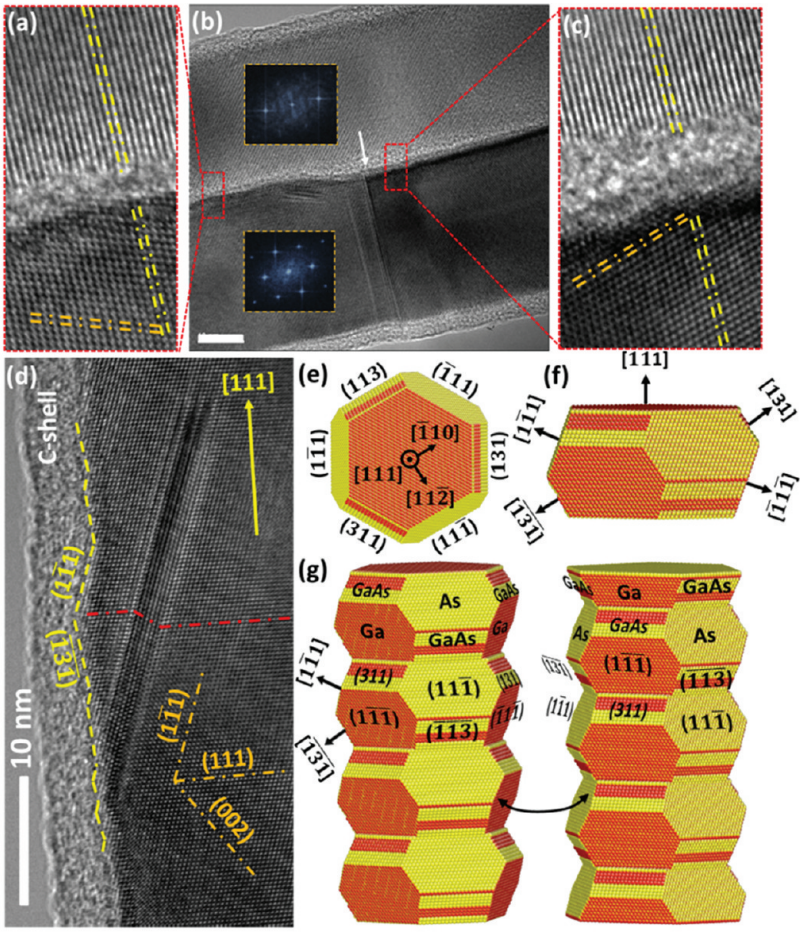

Figure 2. Structural analysis of kissing NWs. (a−c) HRTEM images taken with ⟨110⟩ viewing orientation showing registered (111) planes across the two kissing NWs: (a) before and (c) after the stacking fault marked by the white arrow in (b). Insets in (b) show FFT patterns from the two NWs. Scale bar is 10 nm. (d) HRTEM image of one of the NWs in (b) taken with $[\bar{1}01]$ viewing orientation showing $(1\bar{1}1)$ and $(\bar{1}3\bar{1})$ facets. A surface nucleated twin boundary nucleated on a $(1\bar{1}1)$ plane can also be seen (ref 28). (e−g) Atomic model of a GaAs NWs grown in the [111] orientation. (e) Top and (f) side views from a ⟨110⟩ orientation showing facet edges consistent with those in (d). (g) Adjacent NWs with polar {111} A and B facets attract each other electrostatically.

length scales points to electrostatic forces acting between these polar surfaces on the two NW facets to overcome the mechanical stiffness. Short-range forces acting on the two NWs are small compared to the mechanical forces required for kissing, thus the influence of sintering (due to surface energy minimization), van der Waals, or Casimir forces is negligible.

For NWs to kiss, the gain in electrostatic energy must overcome the mechanical energy required to bend them. Based on the energy balance,[29] one can construct a simple nanobeam model that accounts for the geometrical properties of the NWs and the Coulomb interaction between polar surfaces. The geometrical parameters used to describe the bending force (F) acting on the nanobeam are shown in Figure 3a, where L is the length of the beam, x is the bending displacement (deflection), and y is the integration variable along the beam axis. The nanobeam radius and the distance between two nanobeams are denoted by r and d, respectively. Within the Euler−Bernoulli beam theory,[30] the bending moment $M = -F(L - y)$ is related to the deflection by $M = -EI(d^2x/dy^2)$, where E is the Young modulus and I the area moment of inertia. From this, it is straightforward to show that $x = -FL^3/3EI$. Hence, the total bending energy (E_b) for a system of two NWs can ultimately be expressed as:

$$E_b = 2 \times \int_0^L \frac{M^2}{2EI}\,dy = \frac{15\sqrt{3}Ex^2r^4}{16L^3} \quad (1)$$

where the moment of inertia for a beam with hexagonal cross section is $I = 5\sqrt{3}r^4/16$. The Young modulus of GaAs NWs with different dimensions has been recently determined by in situ compression measurements.[31] For NWs with radius r = 20 nm, the Young modulus was determined to be E = 183 GPa. Using typical values for the NW length of L = 1.6 μm and interdistance d = 0.3 μm (Figure 1c), eq 1 at the point of contact ($x = d/2$) yields $E_b = 2.6 \times 10^{-16}$ J.

The electrostatic energy (E_e) gained by bending two NWs due to the Coulomb attraction between oppositely charged polar microfacets can be estimated from the difference between the Coulomb energy in the initial and final configuration (i.e., before and after bending):

$$E_e = E_{final} - E_{initial} = \frac{-Q^2}{4\pi\varepsilon} \times \left(\sum_{j=1}^{n}\sum_{i=1}^{n}\frac{1}{s_{ij2}} - \sum_{j=1}^{n}\sum_{i=1}^{n}\frac{1}{s_{ij1}} \right) \quad (2)$$

dx.doi.org/10.1021/nl202888e |Nano Lett. XXXX, XXX, 000–000

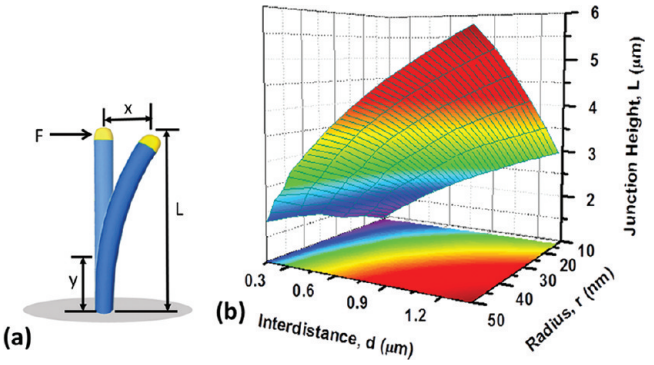

Figure 3. (a) Schematic of the geometrical parameters used to estimate the mechanical bending energy of the nanobeam. (b) Zero total energy surface as a function of NW radius (r), interdistance (d), and height of the junction (L) for a surface density of charges of $n_p \sim 3 \times 10^{12}$ cm^{-2}. Kissing is energetically favorable in the area above the surface, where $E_t = E_e + E_b < 0$.

where ε is the vacuum permittivity, Q is the charge on the A or B polar surfaces (terminated with either Ga or As atoms), each contributing one dangling bond normal to the surface,[32] s_{ij} is the distance between the i-st facet on one side and the j-st facet on the other side at rest, $s_{ij1} = (d^2 + (i-j)^2 \cdot A^2)^{1/2}$, and $s_{ij2} = A \cdot (i^2 + j^2 - 2ij \cos\theta)^{1/2}$ at the point of contact. Here d is the distance between two NWs at rest, and A is the total axial length of the two {111} and {113} facets. The surface density of charges ($n_p = Q/qrA$) can be estimated assuming that the electrostatic attractive energy equals the mechanical bending energy ($|E_e| = |E_b|$) at the point of contact. For typical NW dimensions of $r \sim 20$ nm and $d \sim 0.3$ μm (Figure 1c) and A ~ 16 nm (Figure 2d), this leads to $Q/q \sim 10$ and $n_p \sim 3 \times 10^{12}$ cm^{-2}. This charge density is reasonable, given a spontaneous polarization density of charges of $\sim 10^{13}$ cm^{-2} in polar III−V and II−VI materials.[33,34] Thus, our coupled experiment model does also provide a new method for extracting surface charge densities on polar 3D surfaces, which is usually difficult to measure by other techniques.

To elucidate the dependence of the energetics on the relevant geometrical parameters, Figure 3b shows the zero total energy surface ($E_t = E_e + E_b = 0$) as a function of NW radius (r), interdistance (d) and junction height (L), assuming $n_p \sim 3 \times 10^{12}$ cm^{-2}. Kissing is energetically favorable when the total energy is negative (the region above the zero energy surface), i.e., for small NW radii and distances and for long junctions. Notice that, besides diminishing mechanical stiffness, reduction of r also reduces the amount of the surface charge on the polar surfaces responsible for the electrostatic attraction.

The most convincing evidence that kissing may happen in situ, during the VLS growth, is given by the formation of monolithic Y- and T-junctions. Figure 4 shows the SEM images of a single Y-junction (a) and a single T-junction (b) found upon dispersing the NWs onto a host Si substrate. Kissing leads to the formation of Y-junctions when two vertical NWs growing parallel to each other fuse together (Figure 4a). On the other hand, if the electrostatic attractive force is unbalanced (e.g., for NWs with different diameters), one NW can bend more sharply toward the other, and a T-junction is formed (Figure 4b). HRTEM analysis shows that such monolithic junctions are fully relaxed through the formation of dislocation defects and twin boundaries (Figure 4c). T-junction formation maintains an epitaxial relationship between the two merged NWs (Figure 4c). Interestingly, the

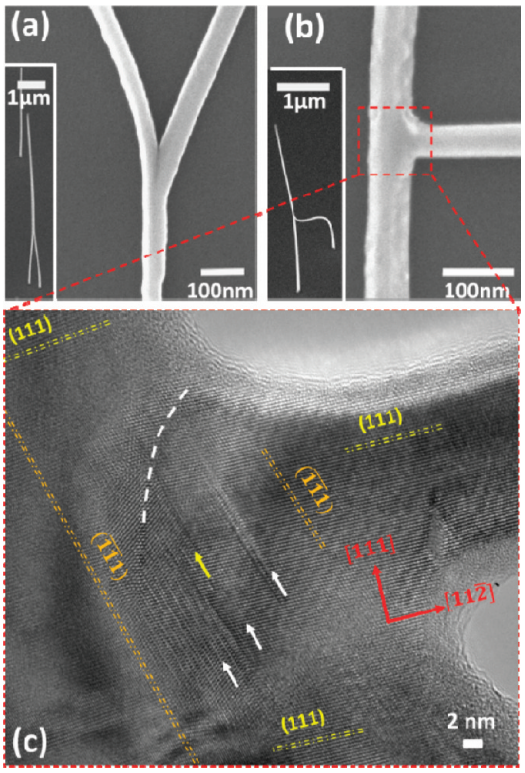

Figure 4. (a and b) Representative SEM images of monolithic junctions found among GaAs NWs dispersed on a host Si substrate: (a) Y- and (b) T-junction. The insets show the different geometries of the NW bundles from which the two types of junctions are thought to originate. (c) HRTEM image of a single crystalline T-junction: (111) planes are continuous throughout the junction, and a slight bend between the thin NW joint and the larger diameter NW is accommodated by stacking faults (white arrows) and a twin boundary (yellow arrow).

smaller diameter NW has a [112] growth orientation in agreement with observations for small diameter group IV NWs.[35] The {111} lattice planes are continuous from the larger to smaller diameter NW in Figure 4c. A slight twist between the two NWs is accommodated by few stacking faults and a twin boundary in the inclined ($\overline{1}11$) planes at the interface between the two NWs. Since the diameter of the larger NW does not change before and after the T-junction, most likely the Au nanoparticle atop the smaller diameter NW diffuses down the larger diameter NW sidewalls; this is consistent with the incerased surface roughness induced on the stem of the larger diameter NW near the T-junction visible in Figure 4b.[36]

Besides its relevance to the fundamental mechanisms governing VLS NW growth, the synthesis of Y- and T-junctions can provide a method for the directed self-assembly of complex hyperbranched architectures in alternative to the reseeding method proposed to realize functional NW circuits and logic elements.[37,38] A similar process was also demonstrated in the case of SiC bi-NWs, where monolithic junctions with plane defects were observed upon merging of two individual NWs growing in a nonvertical orientation relative to the substrate.[39] The understanding gained from the modeling was exploited for the controlled synthesis of vertical Y-junction arrays (Figure 5). An array of Au growth seeds arranged in dimer configuration with large and small (Figure 5a and b insets, respectively) diameters was prepatterned on the GaAs growth substrate by e-beam

dx.doi.org/10.1021/nl202888e |Nano Lett. XXXX, XXX, 000–000

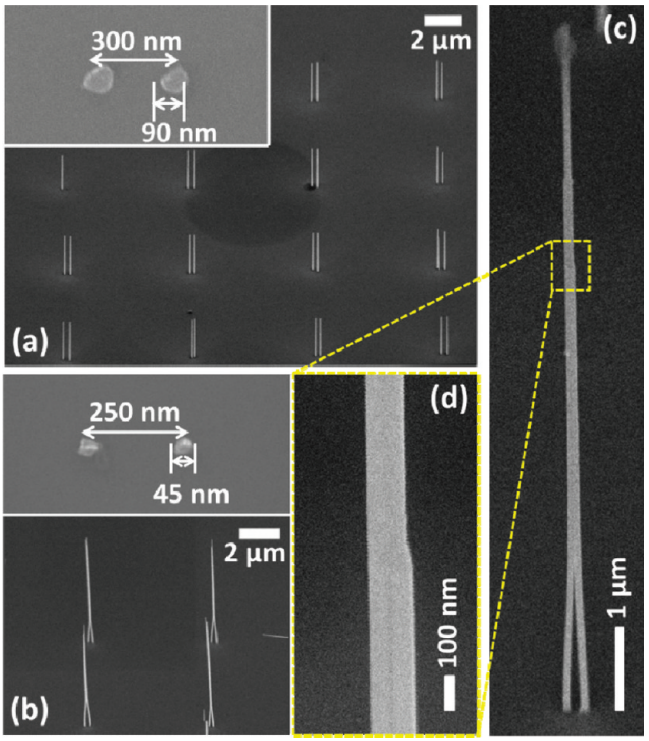

Figure 5. Selective area NW growth from ordered arrays of dimers (a pair of Au nanodiscs) obtained via e-beam lithography patterning. (a) NWs grow parallel and well separated from each other for dimers with large Au nanoparticle size (r = 45 nm) and distance (d = 300 nm). (b) NW kissing is induced by dimers with small nanoparticle size (r = 22.5 nm) and distance (d = 250 nm). The insets of (a) and (b) show the dimers patterned by e-beam lithography before the growth. (c) A vertical monolithic Y-junction formed from the dimer upon merging of two kissing nanowires. (d) A magnified view of the junction in (c) showing the fusion of the two vertical NWs and the subsequent growth of a single stem.

lithography. Upon VLS growth, the first pattern resulted in mechanically robust, vertical NWs, while the second pattern favored kissing of the thin (flexible) NWs kept in close vicinity within the dimer arrangement. It is noteworthy that the smaller size nanoparticles of Figure 5b in closer proximity lead to the growth of longer NWs due to a diffusion limited growth behavior[23] and possible synergetic effects due to NW proximity.[40] Following the mechanism described earlier, in some cases kissing of NWs within the dimer evolves into vertical monolithic Y-junctions formed at the preselected locations. This is shown in the magnified images in Figures 5c and d taken from one of the dimers in the array, where merging of the two original NWs is clearly visible. Near the junction the diameter of the merged NWs increases, consistent with the increase of volume of the fused Au nanoparticles. Further away from the junction, instabilities in the Au nanoparticle and diffusion down the NW stem cause a step-like reduction in the NW diameter and some surface roughness, as evident in Figure 4a (left branch) and Figure 5c.

Preliminary testing of the transport properties of monolithic junctions formed by this method has shown that all branches are electrically connected, hence these structures will be suitable for the realization of junction field effect transistors (J-FETs),[37,41] quantum junctions,[42] or even bioprobes for intracellular sensing.[43] The guided self-assembly of vertical monolithic junctions in selected areas of the substrate demonstrated in this work may therefore be regarded as a viable route toward large-scale integration of vertical arrays of advanced functional NW devices.

In conclusion, the phenomenon of kissing and self-assembly of monolithic junctions has been investigated in GaAs NWs grown by the VLS method. HRTEM analysis was employed to correlate the attractive forces acting on the NWs to the presence of charged polar surfaces inferred from their crystallographic structure. Since {111} polar type facets are commonly found in NWs growing in typical [111], [211], and [110] orientations,[44] kissing is expected to be a rather general phenomenon. The mechanical and electrostatic energy balance for polar NWs in close proximity was calculated within a simple nanobeam model, supporting the experimental observation of GaAs NW kissing and providing general guidelines for the design of dense arrays of vertical polar NWs. The in situ growth of monolithic NW junctions was demonstrated by selective area growth of NW dimers, highlighting the potential of controlling electrostatic interactions to guide the self-assembly of novel functional NW structures.

■ ASSOCIATED CONTENT

Supporting Information. Video shows the merging of two vertical NWs in real time during SEM observation. Figure S1 shows a large-area view of the NW array obtained from the prepatterned Au dimers in Figure 5b. Although the yield of NW dimer nucleation is somehow low leading to single NW growth per dimer as indicated by the white arrow in Figure S1, the yield of bundles formed from NW dimers is close to unity. This material is available free of charge via the Internet at http://pubs.acs.org.

■ AUTHOR INFORMATION

Corresponding Author
*E-mail: csoci@ntu.edu.sg.

■ ACKNOWLEDGMENT

The authors are grateful to Prof. Tang Xiaohong, Dr. Liu Hongbo, and Dr. Haryono Hartono for their assistance with MOCVD operation and for the useful discussions, Prof. Chen Hongyu for the preliminary discussions regarding this work, and Ms. Gwenaelle Vest for assistance with data analysis. Research was supported by the NTU NAP startup grant M58110065, the Funding of Initiatives in Support of NTU 2015 (M58110092), and the MERLION Programme 2010 of the French Embassy in Singapore (dossier no. 2.04.10). Part of this research was conducted at the Center for Integrated Nanotechnologies (CINT), a U.S. Department of Energy, Office of Basic Energy Sciences user facility at Los Alamos National Laboratory (contract DE-AC52-06NA25396).

■ REFERENCES

(1) Timko, B. P.; Cohen-Karni, T.; Quan, Q.; Bozhi, T.; Lieber, C. M. *IEEE Trans. Nanotechnol.* **2010**, *9*, 269–280.
(2) Soci, C.; Zhang, A.; Bao, X.-Y.; Kim, H.; Lo, Y.; Wang, D. *J. Nanosci. Nanotechnol.* **2010**, *10*, 1430–1449.
(3) Ponzoni, A.; Comini, E.; Sberveglieri, G.; Zhou, J.; Deng, S. Z.; Xu, N. S.; Ding, Y.; Wang, Z. L. *Appl. Phys. Lett.* **2006**, *88*, 203101–203103.

(4) Tomioka, K.; Tanaka, T.; Hara, S.; Hiruma, K.; Fukui, T. *IEEE J. Sel. Top. Quantum Electron.* **2010**, *99*, 1–18.
(5) Fan, Z.; Razavi, H.; Do, J.-w.; Moriwaki, A.; Ergen, O.; Chueh, Y.-L.; Leu, P. W.; Ho, J. C.; Takahashi, T.; Reichertz, L. A.; Neale, S.; Yu, K.; Wu, M.; Ager, J. W.; Javey, A. *Nat. Mater.* **2009**, *8*, 648–653.
(6) Verheijen, M. A.; Immink, G.; de Smet, T.; Borgström, M. T.; Bakkers, E. P. A. M. *J. Am. Chem. Soc.* **2006**, *128*, 1353–1359.
(7) Qian, F.; Gradečak, S.; Li, Y.; Wen, C.-Y.; Lieber, C. M. *Nano Lett.* **2005**, *5*, 2287–2291.
(8) Algra, R. E.; Verheijen, M. A.; Borgström, M. T.; Feiner, L.-F.; Immink, G.; van Enckevort, W. J. P.; Vlieg, E.; Bakkers, E. P. A. M. *Nature* **2008**, *456*, 369–372.
(9) Bao, X.-Y.; Soci, C.; Susac, D.; Bratvold, J.; Aplin, D. P. R.; Wei, W.; Chen, C.-Y.; Dayeh, S. A.; Kavanagh, K. L.; Wang, D. *Nano Lett.* **2008**, *8*, 3755–3760.
(10) Dayeh, S. A.; Aplin, D. P. R.; Zhou, X.; Yu, P. K. L.; Yu, E. T.; Wang, D. *Small* **2007**, *3*, 326–332.
(11) Van Tilburg, J. W. W.; Algra, R. E.; Immink, W. G. G.; Verheijen, M.; Bakkers, E. P. A. M.; Kouwenhoven, L. P. *Semicond. Sci. Technol.* **2010**, *25*, 024011.
(12) Wernersson, L. E.; Bryllert, T.; Lind, E.; Samuelson, L. *IEEE Int. Electron Devices Meet., Tech. Dig., 50th* **2005**, 273–276.
(13) Dayeh, S. A. *Semicond. Sci. Technol.* **2010**, *25*, 024004.
(14) Whang, D.; Jin, S.; Lieber, C. M. *Jpn. J. Appl. Phys.* **2004**, *43*, 4465–4470.
(15) Yu, G.; Lieber, C. M. *Pure Appl. Chem.* **2010**, *82*, 2295–2314.
(16) Molares, M. E. T.; Buschmann, V.; Dobrev, D.; Neumann, R.; Scholz, R.; Schuchert, I. U.; Vetter, J. *Adv. Mater.* **2001**, *13*, 62–65.
(17) Mårtensson, T.; Carlberg, P.; Borgström, M.; Montelius, L.; Seifert, W.; Samuelson, L. *Nano Lett.* **2004**, *4*, 699–702.
(18) Ji, R.; Lee, W.; Scholz, R.; Gösele, U.; Nielsch, K. *Adv. Mater.* **2006**, *18*, 2593–2596.
(19) Wagner, R. S.; Ellis, W. C. *Appl. Phys. Lett.* **1964**, *4*, 89–90.
(20) Morral, A. F. *IEEE J. Sel. Top. Quantum Electron.* **2011**, *17*, 819–828.
(21) Liu, J.; Lee, S.; Lee, K.; Ahn, Y. H.; Park, J.-Y.; Koh, K. H. *Nanotechnology* **2008**, *19*, 185607.
(22) Plissard, S.; Larrieu, G.; Wallart, X.; Caroff, P. *Nanotechnology* **2011**, *22*, 275602.
(23) Soci, C.; Bao, X.-Y.; Aplin, D. P. R.; Wang, D. *Nano Lett.* **2008**, *8*, 4275–4282.
(24) Joyce, H. J.; Wong-Leung, J.; Gao, Q.; Tan, H. H.; Jagadish, C. *Nano Lett.* **2010**, *10*, 908–915.
(25) Dayeh, S. A.; Soci, C.; Bao, X.-Y.; Wang, D. *Nano Today* **2009**, *4*, 347–358.
(26) Bhunia, S.; Kawamura, T.; Fujikawa, S.; Nakashima, H.; Furukawa, K.; Torimitsu, K.; Watanabe, Y. *Thin Solid Films* **2004**, *464−465*, 244–247.
(27) Geelhaar, L.; Márquez, J.; Jacobi, K.; Kley, A.; Ruggerone, P.; Scheffler, M. *Microelectron. J.* **1999**, *30*, 393-396.
(28) Dayeh, S. A.; Wang, J.; Li, N.; Huang, J. Y.; Gin, A. V.; Picraux, S. T. *Nano Lett.* **2011**, DOI: 10.1021/nl202126q.
(29) Hill, J. J.; Haller, K.; Gelfand, B.; Ziegler, K. J. *ACS Appl. Mater. Interfaces* **2010**, *2*, 1992–1998.
(30) Beer, F. P.; Johnston, E. R.; DeWolf, J. T. *Mechanics of materials*, 3rd ed.; McGraw-Hill: Boston, MA, 2004.
(31) Wang, Y.-B.; Wang, L.-F.; Joyce, H. J.; Gao, Q.; Liao, X.-Z.; Mai, Y.-W.; Tan, H. H.; Zou, J.; Ringer, S. P.; Gao, H.-J.; Jagadish, C. *Adv. Mater.* **2011**, *23*, 1356–1360.
(32) Haberern, K. W.; Pashley, M. D. *Phys. Rev. B* **1990**, *41*, 3226.
(33) Bernardini, F.; Fiorentini, V.; Vanderbilt, D. *Phys. Rev. B* **1997**, *56*, R10024.
(34) Dayeh, S. A.; Susac, D.; Kavanagh, K. L.; Yu, E. T.; Wang, D. *Adv. Funct. Mater.* **2009**, *19*, 2102–2108.
(35) Schmidt, V.; Senz, S.; Gösele, U. *Nano Lett.* **2005**, *5*, 931–935.
(36) Dayeh, S. A.; Gin, A. V.; Picraux, S. T. *Appl. Phys. Lett.* **2011**, *98*, 163112.
(37) Wang, D.; Qian, F.; Yang, C.; Zhong, Z.; Lieber, C. M. *Nano Lett.* **2004**, *4*, 871–874.
(38) Cheng, C.; Liu, B.; Yang, H.; Zhou, W.; Sun, L.; Chen, R.; Yu, S. F.; Zhang, J.; Gong, H.; Sun, H.; Fan, H. J. *ACS Nano* **2009**, *3*, 3069–3076.
(39) Cuilan, W.; Xiaozhou, L.; Jianghua, C. *Nanotechnology* **2010**, *21*, 405303.
(40) Borgström, M. T.; Immink, G.; Ketelaars, B.; Algra, R.; Bakkers, E. P. A. M. *Nat. Nanotechnol.* **2007**, *2*, 541–544.
(41) Do-Hyun, K.; Jun, H.; Rao, B. K.; Wonbong, C. *IEEE Trans. Nanotechnol.* **2006**, *5*, 731–736.
(42) Chen, S.; Trauzettel, B.; Egger, R. *Phys. Rev. Lett.* **2002**, *89*, 226404.
(43) Tian, B.; Cohen-Karni, T.; Qing, Q.; Duan, X.; Xie, P.; Lieber, C. M. *Science* **2010**, *329*, 830–834.
(44) Hanrath, T.; Korgel, B. A. *Small* **2005**, *1*, 717–721.